McCoy, S.W., Coe, J.A., Kean, J.W., Tucker, G.E., Staley, D.M., and Wasklewicz, T.A., 2011, Observations of debris flows at Chalk Cliffs, Colorado, U.S.A.: part 1, in situ measurements of flow dynamics, tracer particle movement and video imagery from the summer of 2009, In Genevois, R., Hamilton, D.L., and Prestininzi, A, eds., Proceedings of the 5th International Conference on Debris Flow Hazards Mitigation, Mechanics, Prediction and Assessment, Padua, Italy, June 14-17, 2011, Italian Journal of Engineering Geology and Environment and Casa Editrice Universita La Sapienza, Rome, Italy. DOI: 10.4408/IJEGE.2011-03.B-078

Authors Note: This paper was presented at the conference, but, due to an error by the publisher, was not printed in the proceedings book. Instead, part 2 by Staley et al. was printed twice. This paper by McCoy et al. is listed in the table of contents as being printed on pages 715-724. The DOI listed above was printed on p. 715.

OBSERVATIONS OF DEBRIS FLOWS AT CHALK CLIFFS, COLORADO, USA: PART 1, IN SITU MEASUREMENTS OF FLOW DYNAMICS, TRACER PARTICLE MOVEMENT AND VIDEO IMAGERY FROM THE SUMMER OF 2009.

MCCOY S.W. (*), COE J.A. (**), KEAN J.W. (**), TUCKER G.E. (*), STALEY D.M. (**) , WASKLEWICZ T.A. (***)

(*) CIRES & Department of Geological Sciences, University of Colorado, Boulder, Colorado 80309, USA. scott.mccoy@colorado.edu
(**) U.S. Geological Survey, Denver Federal Center, MS 966, Denver, Colorado 80225, USA.
(***) Department of Geography, East Carolina University, Greenville, North Carolina 27858, USA.

ABSTRACT

Debris flows initiated by surface-water runoff during short duration, moderate- to high-intensity rainfall are common in steep, rocky, and sparsely vegetated terrain. Yet large uncertainties remain about the potential for a flow to grow through entrainment of loose debris, which make formulation of accurate mechanical models of debris-flow routing difficult. Using a combination of in situ measurements of debris-flow dynamics, video imagery, tracer rocks implanted with passive integrated transponders (PIT) and pre- and post-flow 2-cm resolution digital terrain models (terrain data presented in a companion paper in this volume by Staley *et al*.), we investigated the entrainment and transport response of debris flows at Chalk Cliffs, CO, USA. Four monitored events during the summer of 2009 all initiated from surface-water runoff, generally less than an hour after the first measurable rain. Despite reach-scale morphology that remained relatively constant, the four flow events displayed a range of responses, from long-runout flows that entrained significant amounts of channel sediment and dammed the main-stem river, to smaller, short-runout flows that were primarily depositional in the upper basin. Tracer-rock travel-distance distributions for these events were bimodal; particles either remained immobile or they travelled the entire length of the catchment. The long-runout, large-entrainment flow differed from the other smaller flows by the following controlling factors: peak 10-minute rain intensity; duration of significant flow in the channel; and to a lesser extent, peak surge depth and velocity. Our growing database of natural debris-flow events can be used to develop linkages between observed debris-flow transport and entrainment responses and the controlling rainstorm characteristics and flow properties.

Key Words: debris flow, initiation, entrainment, sediment transport, monitoring, instrumentation, runoff, tracer particles

INTRODUCTION

Debris flows are rapidly gaining recognition as a serious hazard to expanding development, as important agents of mountain landscape evolution, and as a significant mode of sediment transport to rivers in rugged terrain. This recognition has made apparent the need for complete and quantitative datasets from well-constrained natural debris flows to test theoretical and computational approaches, confirm experimental results and stimulate new ideas.

In steep, rocky, and sparsely vegetated terrain, debris flows initiated by surface-water runoff in response to short duration, moderate- to high-intensity rainfall are common (e.g. FRYXELL & HORBERG, 1943; WOHL & PEARTHREE, 1991; MEYER *et al*., 1995; CANNON *et al*., 2001; BERTI & SIMONI, 2005; LARSEN *et al*., 2006; COE *et al*., 2008). Runoff-initiated debris flows can form from small quantities of rain, with very short lag times from the beginning of the rainstorm to the beginning of the debris-flow event (BERTI *et al*., 2000). They start as water-rich flows that rapidly entrain and concentrate large quantities of debris and sediment into hazardous debris-flow fronts (COE *et al*., 2008) and can have peak discharges many times that of a comparable water-flood (VANDINE, 1985). Yet, for this type of debris flow, large uncertainties remain about the mechanics of initiation and the potential for a flow to grow through entrainment of loose debris. These uncertainties make it difficult to formulate accurate mechanical models of debris-flow initiation, routing, and deposition in natural settings and thereby add large uncertainties to hazard assessments.

To relate the entrainment and transport response of a debris-flow event to potential controlling factors such as physical flow properties, rainstorm characteristics, and basin topographic parameters we used a combination of in situ measurements of debris-flow dynamics, video imagery, tracer rocks implanted with passive integrated transponders (PIT) and pre- and post-flow 2-cm resolution digital terrain models acquired through terrestrial laser scanning (TLS). Terrain data are presented in a companion paper in this volume by Staley *et al.*. This combination of readily available technologies captured a comprehensive record of the four debris-

flow events that occurred during the summer of 2009 in a natural debris-flow basin at Chalk Cliffs, Colorado, USA. We documented the initial and final topographic state, the hydrologic conditions leading up to the event, net transport distances of tracer particles and continuous time series of physical flow properties and flow dynamics for each debris-flow event.

In this paper and the companion paper by Staley *et al*. (this volume), we compare the four debris-flow events that occurred during the summer of 2009 (2 June, 26 July, 6 September, 15 September) to highlight dramatic differences in entrainment and transport behavior possible from a single basin with similar topographic initial conditions for each event, yet driven by rainstorms of different intensities and durations.

CHALK CLIFFS STUDY SITE

CATCHMENT DESRIPTION AND GEOLOGIC SETTING

The Chalk Cliffs study area is located on the southern flank of Mount Princeton in the Sawatch Range of Central Colorado, USA. The steep, 0.3 km^2 semi-arid basin is incised into pervasively fractured and hydrothermally altered quartz monzonite, adjacent to the range-bounding Sawatch normal fault (MILLER, 1999). The steep headwaters of the basin are exposed bedrock (generally > 45°) (Fig. 1A). Unconsolidated colluvium and debris-flow deposits (0°-45°) cover the remaining 40% of the basin (COE *et al.,* 2008). Between debris-flow events dry ravel from the steep colluvium and rock fall from the bedrock cliffs rapidly fill the channels with debris. Bedrock slopes in the basin are devoid of vegetation, and colluvial slopes are sparsely vegetated. This basin has a high frequency of debris flows (one to four events per year between the months of May and October) generated by rainfall related surface-water runoff (COE *et al.,* 2008), making it ideal for long-term monitoring. Basin topographic characteristics are summarized in Table 1. A more complete description of the geologic setting and site selection can be found in earlier work (COE *et al.,* 2008, COE *et al.,* 2010).

MONITORING SYSTEM

The automated monitoring system, established through collaboration between the U.S. Geological Survey and the University of Colorado, consists of three instrumented cross sections (upper, middle and lower stations) and two video cameras filming at 2 frames per second (one filming the middle station, the other filming the upper station) (Fig. 1A-D and H). The upper station is located in the west channel, 38 m above the junction with the east channel and ~590 m downstream from the drainage divide. The middle station is 92 m downstream of the upper station and 54 m downstream of the east-west channel junction. The lower station is 319 m downstream of the middle station and is 220 m from the mouth of the basin and the apex of the depositional fan (Fig. 1H).

Table 1. Chalk Cliffs study basin topographic characteristics at each monitoring station shown in Fig. 1A and H. The Chalk Creek location is on the fan where the debris-flow channel enters Chalk Creek (not a station). Elevation, slope, and length parameters correspond to the west channel profile in Figure 1H (inset). Local slopes at the stations were taken over 10-horizontal meters.

	Upper station	Middle station	Lower station	Chalk Creek
Contributing area (km^2)	0.0619	0.1592	0.2426	0.4293
Max. elevation (m)	3100	3100	3100	3100
Station elevation (m)	2780	2750	2690	2520
Mean channel slope (°)	35	32	26	16
Station local channel slope (°)	13	15	8	7
Upslope channel length (m)	586	678	997	2194

As of May 2009 each station was equipped with: an ultrasonic stage sensor (accuracy +/- 1 cm) suspended over the channel to measure the sediment and/or flow height above a fixed datum (the datum is the stable bedrock channel at the upper and middle stations and a buried pressure transducer at the lower station); one or two unvented pressure transducers (accuracy +/- 3 mm water pressure head) to measure the pore-fluid pressure at the bedrock-sediment interface (upper and middle stations) or at ~ 0.25 m depth in the bed sediment (lower station); a siphoning rain gauge (accuracy +/- 2%); and a temperature sensor (see MCCOY *et al.,* 2010 for complete sensor specifications). All these sensors were sampled every 2 seconds during a rainstorm.

At the upper station only, we mounted a 15.24 cm by 15.24 cm (232 cm^2) metal plate attached to a single-axis load cell (accuracy +/- 2.5 kg) flush with the bedrock channel to measure total normal stress at the sediment-bedrock interface. This load cell was sampled at 250 Hz through June 2009; we subsequently reduced the sampling rate to 100 Hz. Additional measurements of rainfall and soil moisture (accuracy +/- 5% volumetric water content) were made on adjacent hillslopes within the basin and within the channel below the middle station.

Near-realtime data and a daily photograph from the upper station were sent to a web server using a cell phone modem. This system allowed us to know when a debris-flow event had occurred (http://landslides.cr.usgs.gov/monitoring/chalk_cliffs/index.php).

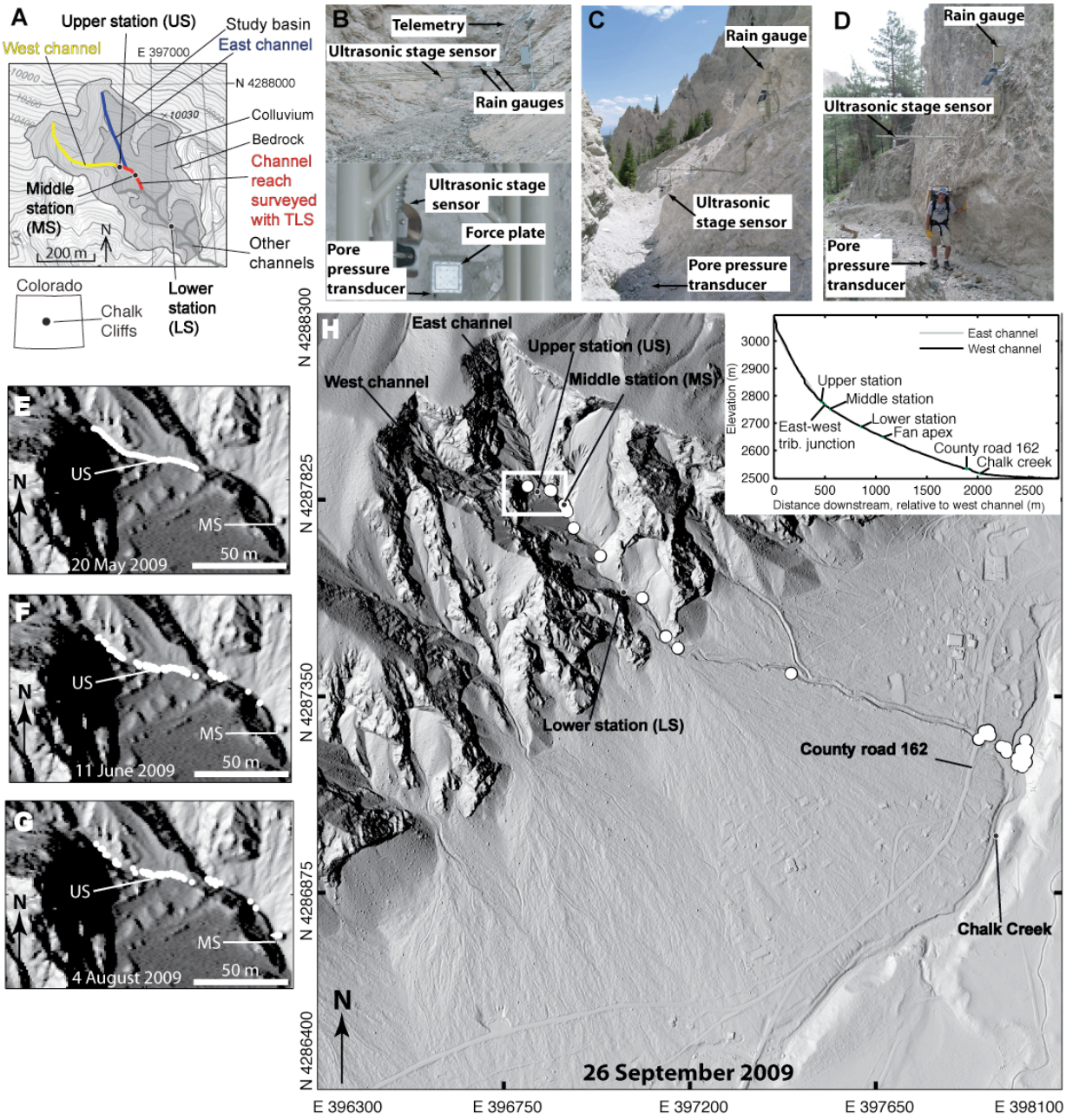

Fig.1.Chalk Cliffs study area with photographs of the monitoring stations and shaded relief images (from 1 m ALSM data provided by NCALM) with tracer-particle positions marked by white circles. White rectangle in H encompasses zoomed-in view shown in E, F, and G. A) Line drawing of study basin showing station locations and the distribution of bedrock and colluvium (redrawn from MCCOY et al., 2010) B) Upper station with sensors. C) Middle station. D) Lower station. E) Starting tracer-particle positions 20 May 2009. F) Positions 11 June 2009, 9 days after 2 June 2009 event. G) Positions 4 August 2009, 9 days after 26 July 2009 event. H) Positions 26 September 2009, 11 days after 15 September 2009 event (note no survey was completed after the 06 September 2009 event). Inset: Long profile of east and west channel.

METHODS

TRACER ROCKS

We implanted 32-mm passive integrated transponders (PIT) in 99 rocks to measure the travel distances of cobbles during a debris-flow event. PIT tags "labelled" each rock with a unique identification number. Using radio-frequency identification (RFID) technology, we could find and identify these tracer rocks, buried up to ~ 0.25-0.5 m depth, without disturbing the bed surface (BRADLEY, 2010). We selected the tracer rocks from the area surrounding the upper station. Rock strength determined the size of selected rocks; rocks that were too small broke when drilled with the hammer drill. The mean length of the a, b, and c axes of the tracer rocks were 13 cm, 9 cm, and 6 cm, respectively. For comparison, the mean length of the a, b, and c, axes of 100 randomly selected rocks from an October 2008 debris-flow deposit forming the levees and bed at the upper station were 10 cm, 7 cm, and 4 cm, respectively. We prepared the tracer rocks by drilling a 4.76 mm diameter hole with a hammer drill, inserting a 32 mm long PIT tag and then sealing the hole with marine epoxy. To aid in the recovery of surface rocks and the initial survey, we spray-painted all tracers red. We then placed the rocks in groups of three, along the centerline of the channel, in the reach by the upper station, with each group separated by ~2 m (Fig. 1E), and surveyed their positions using a total station.

After each debris-flow event, we searched the entire travel-path of the debris flow using a 0.5 m diameter RFID detection antenna. When a tracer rock was passed over by the antenna, the capacitor in the PIT tag was charged, which enabled the tag to transmit its unique identification number to the receiver to be recorded. Once the tracer rock was recorded, we surveyed its location using a total station. Many of the tracer rocks were buried below the deposit surface and never visually identified. The resulting error, +/- ~0.5 m, in the surveyed position was primarily due to the read-range of the antenna.

To measure the total curvilinear distance travelled (streamwise and cross-stream) by a tracer rock during a single debris-flow, we projected tracer-particle positions onto the longitudinal profile of the debris-flow channel. The longitudinal profile was extracted from a 1 m digital elevation model derived from airborne laser swath mapping (ALSM) data collected by the National Center for Airborne Laser Mapping (NCALM). We then calculated along slope travel distance by differencing the post-event and pre-event slope distance along the longitudinal profile. All tracer rocks that moved less than 1 m were put in the 1 m bin for plotting on the log-log scale in Fig. 2.

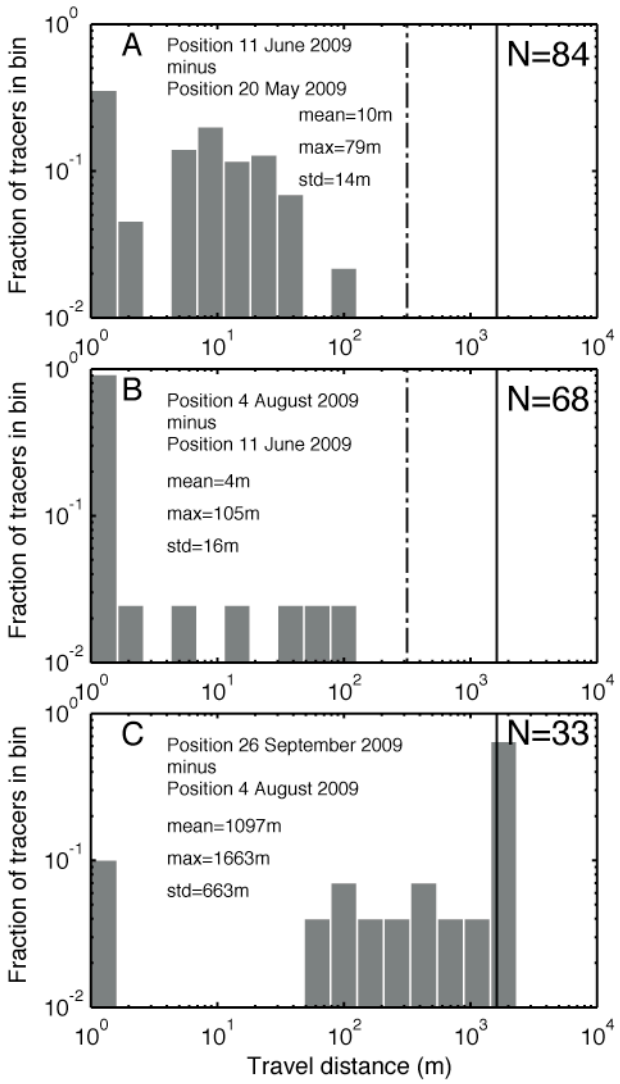

Fig.2. Histograms of tracer-particle travel distance between consecutive surveys. Solid line is the travel distance from the mean starting position on 20 May to the junction with the perennial stream Chalk Creek. Dashed line is the distance travelled by the flow front. In C, both lines overlap. A) Distance travelled due to 2 June 2009 event. B) Distance travelled due to 26 July 2009 event. C) Distance travelled due to combination of 6 September 2009 and 15 September 2009 events.

STATION-DATA PROCESSING

To remove much of the +/- 2.5 kg noise in the force time series, we downsampled the 250 Hz and 100 Hz force plate data to 10 Hz by binning data in 0.1 s bins and taking the mean of each bin. The stress axis in Figs. 3-6 was scaled such that stage H and basal stress σ superpose if $\sigma = \rho g H \cos(\theta)$ with ρ=2040 kg/m^3, where ρ is the wet bulk density of the sediment bed and flow combined, g is the gravitational acceleration, H is the bed-normal height of material above the force plate, equal to stage, and θ is the bed inclination (i.e., σ plots above H when ρ_{actual}>2040 kg/m^3 and σ plots below H when ρ_{actual}<2040 kg/m^3). Note that accurate bulk densities can only be determined from this method when the assumption of a lithostatic stress state is valid.

The load cell was buried beneath sediment for the majority of 2009, which precluded taking a new tare value before each event. To minimize error associated with a tare value that is a function of environmental factors (primarily temperature), we took advantage of the fact that before rainstorms the bed sediment was dry (~10% volumetric water content) and thus should have a relatively constant bulk density before each event. We set the force tare value using a pre-storm dry bed sediment bulk density of 1750 kg/m3; this value was determined just after installation. We estimated the approximate uncertainty resulting from this assumption as +/- 100 kg/m^3 or +/- 500 Pa if 0.5 m of sediment is present.

We filtered the 2 s ultrasonic stage data based on echo return strength to remove low strength returns. Persistent increases or decreases in stage were due to sediment deposition or erosion.

To measure pore-fluid pressure using the unvented, temperature-compensated pressure transducers, we subtracted the pre-storm pressure (i.e., atmospheric pressure) from the total pressure. For most of the events, the bed sediment between the flow and the pressure transducer was not saturated. Given these conditions, the pressure transducer did not measure positive pressure head due to the overriding flow (not shown in our figures) or the pressure head was attenuated. The only exception to these behaviours was recorded at the middle station on 2 June.

We calculated surge front velocities (each event was composed of multiple surge fronts) by manually tracking surge front positions in the spatially referenced video imagery recorded by the upper station camera. Surge-front velocities $\overline{u}$ were then plotted as a function of maximum surge depth h to develop a rating curve for the upper station ($\overline{u} = 3.6h^{1/2}$). To calculate maximum flow depth, the height of the bed sediment and the maximum stage during the surge must be known. We used the period of no or little flow in between successive surges to determine the bed height through time. We automated this procedure by taking a moving-window minimum of the stage data, with a window width equal to the maximum surge duration for each event. It has been demonstrated by others (PIERSON, 1986; SUWA *et al*., 1993; ARATTANO *et al*., 2000) that the peak flow velocity can occur after the peak flow depth and coarse-grained flow front have passed. Since many of the surges were of short duration and we only measured the surge front velocities, we did not detect this phenomena, but if present, it would make our rating curve underestimate the actually velocities in the more shallow, dilute portions of the surge.

For each debris-flow event, we calculated an estimate of the total event volume passing the upper station (sediment plus water) using $Vol = \sum_{t_i}^{t_f} \overline{u}(h(t))A(t)\Delta t$, where the summation was taken from the beginning of the flow event t_i to the end t_f, $\overline{u}$ is the mean cross sectional velocity from the rating curve, $A(t)$ is the current active cross sectional area at a given time calculated using the surveyed bedrock cross section, the current bed height, and current flow depth, and Δt is the length of time between two stage measurements (typically 2 s).

To determine the total time spent above certain transport stages during the coarse of a debris-flow event we summed the total time over which the flow depth was greater than 0.1 m, 0.2 m, and 0.3 m.

RESULTS AND DISCUSSION

Monitoring results from the four debris-flow events indicated that 2 June and 26 July events had relatively short travel distances, stayed within the basin and were primarily depositional in nature. In sharp contrast, the 15 September event was primarily erosional in nature and traveled all the way to the modern fan at Chalk Creek, where it temporarily dammed the stream. The 6 September event was intermediate to these two end members, exiting the basin, but not reaching Chalk Creek. Below, we first provide details on the tracer-particle travel distance distributions and then describe the conditions that caused this dramatic difference in entrainment and transport behavior between the 4 events.

TRACER ROCKS

Of the initial 99 PIT-tagged tracer rocks (Fig. 1E), the number of tracer rocks with known pre-event and post-event positions was 84, 68, and 33 after the 2 June, 26 July, and 15 September events,

respectively. We were not able to conduct a survey after the 6 September event do the rapid arrival of the 15 September event. These recovery rates are much smaller than those obtained using the same techniques and technology in a fluvial environment, where the rates can be up to 98% (BRADLEY, 2010). At Chalk Cliffs, the high losses were due to burial of many of the tracers, especially in the 15 September event, to depths greater than the read range of the antenna (~0.25-0.5 m).

In our early surveys, we found most of the tracer rocks in the seed reach near their origins (Fig.1 E-G). However, our final survey on 26 September 2009, following the 15 September event, showed that the highest concentration of tracer rocks had shifted ~1.6 km downstream to the fan at the junction of the debris-flow channel and the perennial stream Chalk Creek (Fig. H). The 6 September event did not reach county road 162 (Fig. 1H), however 67% of tracer particles were found below the road on 26 September. Because extended sediment transport was due to the 15 September event, and only small amounts of erosion were measured at the monitoring stations after the 6 September event (Fig. 5), we grouped the 6 September event with the earlier lower-transport events.

The fraction of particles that moved greater than 1 m after the 2 June, the 26 July, and the 15 September events were 67%, 25% and 94%, respectively. Distributions of travel distance are plotted in Fig. 2 and summarized in Table. 2. Travel distances measured after the 2 June event and the 26 July event (Fig. 2A and B) differ greatly from the distribution for the 15 September event (Fig. 2C). Travel distances < 1 m dominate the distributions for the low transport events (Fig. 2A and B), whereas travel distances > 1500 m dominate the distribution for the 15 September event (Fig. 2C).

The maximum possible travel distance for a tracer particle transported by a debris flow is set by its starting position and the downstream end of the debris-flow dominated portion of the catchment, which in this case is near the junction of the debris-flow channel and the perennial stream Chalk Creek (which flows down a low-gradient glacial valley). The distance from the mean tracer starting position on 20 May to the end of the debris-flow dominated system (the junction of the debris-flow channel and Chalk Creek) was 1620 m. For the 2 June and 26 July events, the mean travel distances were 10 m and 4 m, or only 0.6% and 0.2% of the channel length dominated by debris flows. The mean tracer travel distance was also considerably shorter than the maximum flow-front travel distance for these two flows, which was on the order of 300 m. In contrast, the mean tracer travel distance for the 15 September event, which had a maximum flow-front travel distance of 1620 m, was 1100 m or 68% of the 1620 m debris flow dominated channel length. Sixty-seven percent of the recovered population travelled a distance equal to the debris flow dominated channel length in one event. Moreover, both the mean travel distance of 1100 m and the percent of particles that travelled the entire length of the debris flow dominated channel length are underestimated for the 15 September event due to undercounting of tracer particles. Upstream of the fan, few debris-flow deposits had depths greater than the read range of the antenna (STALEY *et al*., this volume), whereas the reach from county road 162 to Chalk Creek had significant areas of aggradation greater than 2 m. Had all particles been found, the measured 15 September distribution would be even more heavily skewed toward travel distances closer to the length of the debris flow dominated portion of the catchment.

Travel-distance distributions were bimodal: particles either remained nearly immobile or they travelled the entire length of the debris flow dominated portion of the catchment (Fig. 2). Although we only have tracer data from three events, if this bimodal distribution is characteristic of travel distances for particles transported by debris flows, it sets them apart from many other modes of sediment transport, in which the single-event travel distance is often a small fraction of the system size (BRADLEY, 2010). The existence of particle travel distances that are equal to the system size calls into question the ability to write sediment transport equations that depend only on local topographic and flow parameters (TUCKER & BRADLEY, 2010).

STATION DATA

Monitoring station data for the four debris-flow events are shown in Figs. 3-6. Key storm characteristics, flow properties, and tracer travel distances are summarized in Table. 2. By comparing the measured rainfall and flow properties between the four 2009 events, we can gain insight into why the September 15 flows were so much more effective, in terms of travel distance, clast transport, and bed entrainment, than the previous three events.

RAINFALL

Cumulative rainfall amounts since the beginnings of each debris-flow producing storm event are plotted as a dashed line in panel A of Figs. 3-6. On the upper axis of panel A in Figs. 3-6, 10-minute

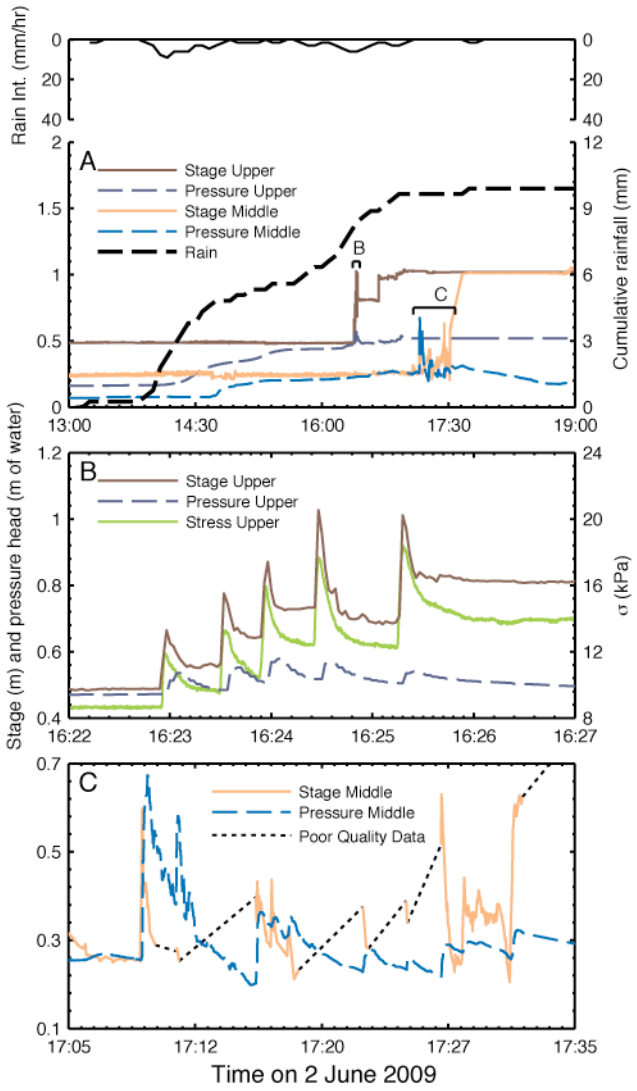

Fig.3. Sensor data 2 June 2009. A) Upper axis: 10-minute rainfall intensities measured at the upper station. Lower axis: Complete event duration measured at the upper and middle station. Flows stopped upstream of the lower station. The first debris flows initiated in the west channel, arrived at the upper station at 16:22:54 and stopped before reaching the middle station. The second set of debris flows initiated in the east channel and arrived at the middle station at 17:09:14. Pre-flow sediment depth at the upper station was 0.47 m and 0.26 m at the middle station. Net change in sediment depth was +0.54 m and +0.78 m at the upper and middle station, respectively. Due to rain at 11:00, pre-event pore pressures were not zero. B) 5-minute time slice encompassing the arrival of the first 5 debris-flow surges at the upper station. C) 20-minute time slice from the middle station.

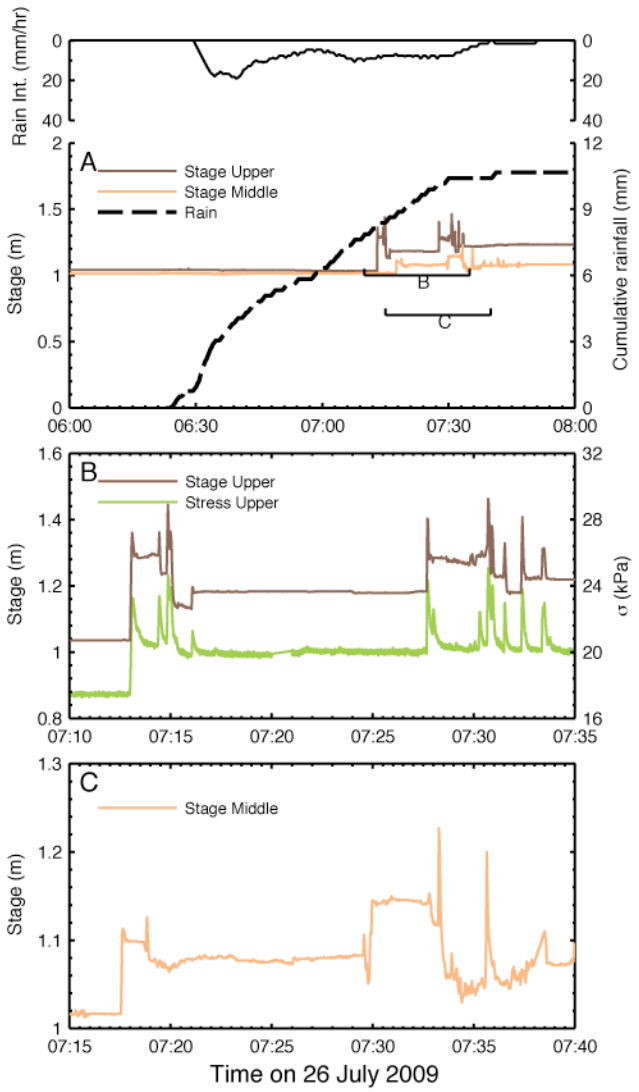

Fig.4. Sensor data 26 July 2009. A) Upper axis: 10-minute rainfall intensities measured at the upper station. Lower axis: Complete event duration measured at the upper and middle station. Flows stopped upstream of the lower station. The first surge front reached the upper station at 7:12:42 and the middle station at 7:17:32. Pre-flow sediment depths at the upper and middle stations were 1.04 m, and 1.01 m, respectively. Net changes in sediment depth at the upper and middle stations were +0.19 and +0.07 m, respectively. B) 25-minute time slice from the upper station. C) 25-minute time slice from the middle station.

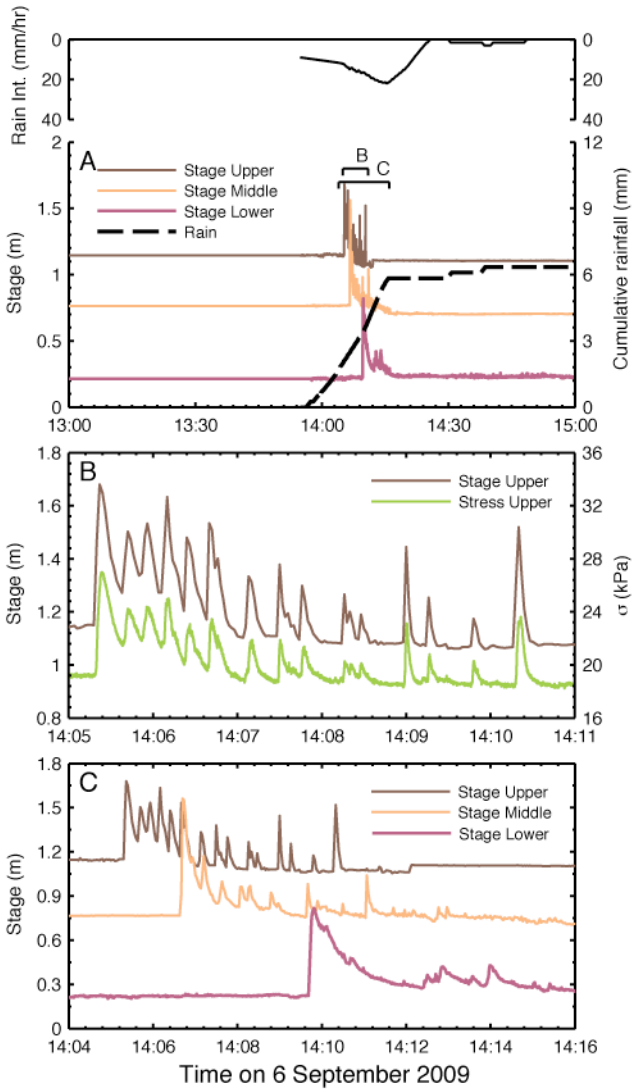

Fig.5. Sensor data 6 September 2009. A) Upper axis: 10-minute rainfall intensities measured at the upper station. Lower axis: Complete event duration measured at the upper, middle and lower stations. Stage at middle station shifted -0.3 m in all plots. The first surge front reached the upper, middle and lower stations at 14:05:18, 14:06:38, and 14:09:41, respectively. Pre-flow sediment depths at the upper, middle and lower stations were 1.14 m, 1.06 m, and 0.22 m, respectively. Net change in sediment depth at the upper, middle and lower stations were -0.04 m, - 0.06 m, and 0.0 m, respectively. B) 6-minute time slice from the upper station. C) 10-minute time slice from the upper, middle and lower stations.

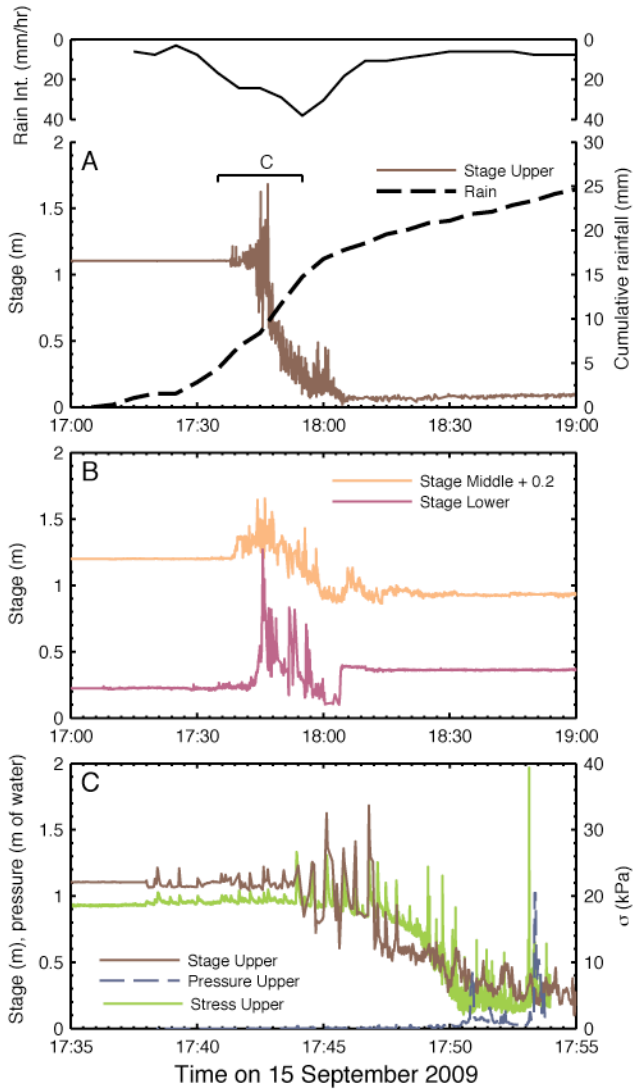

Fig.6. Sensor data 15 September 2009. A) Upper axis: 10-minute rainfall intensities measured at the upper station. Lower axis: Complete event duration measured at the upper station. B) Complete event duration measured at the middle and lower stations. Stage at middle station shifted +0.2 m. The first surge front reached the upper, middle and lower stations at 17:38:18, 17:38:40, and 17:42:41, respectively. Pre-flow sediment depths at the upper, middle and lower stations were 1.1 m, 1.0 m, and 0.22 m, respectively. Net changes in sediment depth at the upper, middle and lower stations were -1.1 m, -0.28 m, and +0.14 m, respectively C): 20-minute time slice from the upper station.

rainfall intensities are plotted. With exception of the 2 June event, all storms had durations less than 2 hours. The 15 September event had the largest cumulative storm rainfall (24.6 mm) and the highest peak 10-minute intensity (38.1 mm/hr). The 6 September event had the smallest storm total (6.3 mm), and the 2 June event had the lowest peak 10-minute intensity (9.1 mm/hr). The first debris-flow surge generally reached the upper station in less than 45 minutes after the onset of rain. There was a poor correlation in time between the storm maximum 10-min intensity and flow initiation, but a tight correlation, often less than a few minutes, with local peaks in 10-minute rainfall intensity and flow initiation (Figs. 3-6). The short temporal lag between the beginning of rain and the first debris-flow surge (as short as 10 minutes) and the close correlation in time with local peaks in the 10-minute rainfall intensity reinforce the role of surface-water runoff as the debris-flow generation process, as opposed to longer response time, infiltration related, land sliding. Similar short response times from the beginning of rain to the initiation of a debris flow have been observed at other field sites (e.g. BERTI *et al*., 2000)

To quantify the role of cumulative rainfall in determining event volume, we normalized the event volume (sediment plus water) measured at the upper station by total rain volume that fell upstream of the upper station (calculated as the product of upstream accumulation area and measured rainfall). This ratio was not constant (range of 6% to 57%) with the large 15 September event having a ratio of 54% and the smallest (2 June event) having 6% (Table. 2). During small flow events, a larger part of the water potentially available for overland flow and debris transport was not measured. In larger events, a greater part of available water passed the station as surface flow of measurable depths, often as debris flows or water-dominated flow vigorously transporting sediment.

VIDEO OBSERVATIONS

Although each debris-flow event varied in size and duration, all events consisted of multiple surges with distinct longitudinal sorting of sediment grainsize. Each surge began with a steep and deep granular front, composed of boulders and other coarse-grained material (often without visible interstitial fluid), which was followed by a shallower, water-rich tail of relatively fine-grained material. The finer-grained tail rapidly changed from a mud-rich slurry of intermediate thickness with a moderate concentration of visible coarse-surface clasts directly behind the granular front, to a shallow, water-dominated, turbulent flow in which intense bed load transport was evident. The duration and depth of the water-dominated tail flows varied greatly. In small events like that of 2 June, the water-dominated flow between surge fronts was a trickle, compared to the 15 September event in which the water-dominated flow vigorously transported sediment between surge fronts and continued transporting and eroding sediment for tens of minutes after the last well-developed granular surge front had passed. Flow front velocities measured at the upper station had a well-defined $h^{1/2}$ scaling, and were best fit by $\overline{u} = 3.6h^{1/2}$. We measured maximum front velocities of 3.7 m/s during the 15 September event.

STAGE

Stage data from the upper, middle and lower stations are shown in Figs. 3-6 for all four events. Neither the 2 June event nor the 26 July event reached the lower station. Both of these events had maximum flow depths < 0.35 m at the upper and middle stations and peak discharges at the upper station less than 2 m^3/s. The two events that travelled past the lower station, 6 September and 15 September, had maximum flow depths >= 0.45 m at the upper and middle stations and peak discharges at the upper station > 5 m^3/s. Peak flow depth of the 15 September event was not consistently larger than the 6 September event (Table. 2).

Sediment deposition occurred at the upper and middle station during the short-runout flows of 2 June and 26 July (Table 2). In contrast, the 6 September event eroded the bed slightly (<= 0.08 m) at the upper and middle stations. The 15 September event eroded to bedrock at the upper station (1.1 m) and eroded significantly at the middle (0.34 m) and lower stations (0.11 m).

The volume (both sediment and water) of each flow measured at the upper station varied significantly between the long-transport 15 September event and the other shorter-transport events. The 15 September event had an event volume at the upper station of ~820 m^3, which was ~4 to 23 times larger than the other events (Table 2). Note that these volumes are not totals for each event because material from the other main tributary (east channel) joins the west channel down slope of the upper station. We did not calculate volumes at the middle station because the poor spatial referencing of video imagery there precluded accurate velocity measurements.

Table. 2 Summary of rainstorm characteristics, flow properties, and tracer travel distances for the four debris-flow events in 2009. Front velocities measured from video at the upper station are denoted with Vus. Front velocities calculated from travel time between the middle station and the upper station are denoted with Vtt. US, MS, LS are upper station, middle station and lower station, respectively.

Event date; time of flow front arrival at US	Cum. rain (mm)	Rain storm duration (min)	Event volume at US (m^3)	Peak discharge at US (m^3/s)	Event volume / Rain volume at US (%)	Duration of flow at (US, MS) with depth> 0.1 m; 0.2 m; 0.3 m (min.)	Max Front velocity Vus; Vtt (m/s)	Max flow depth US; MS; LS (m)	Min; max; mean soil moisture (%)	Event bed height change US; MS; LS (m)	Percent mobile tracers (%)	Max; mean; std tracer travel distance (m)
2 June 2009; 16:22:54	9.9	300	35	1.6	6	(0.8, 4.0); (0.2, 1.0); (0.03, 0.8)	.3; NA	0.31; 0.34; NA	15.5; 18.4; 16.3	+0.54; +0.81; NA	67	79; 10; 14
26 July 2009; 7:12:42	10.7	78	97	2.0	15	(1.5, 0.1); (0.7, 0.0); (0.07, 0.0)	NA; NA	0.32; 0.16; NA	11.7; 11.7; 11.7	+0.19; +0.07; NA	25	105; 4; 16
6 Sept. 2009; 14:05:18	6.3	45	223	5.2	57	(2.1, 1.5); (1.4, 0.7); (0.7, 0.4)	NA; 1.8	0.53; 0.80; 0.60	10.3; 10.3; 10.3	-0.04; -0.06; 0.0	NA	NA
15 Sept. 2009; 17:38:18	24.6	115	822	13.5	54	(9.9, 18.9), (4.7, 6.4), (2.1, 1.2)	3.7; 1.2	1.1; 0.45; 1.02	10.2; 10.8; 10.5	-1.1; -0.28; +0.14	94	1663; 1097; 663

The total length of time that the measured flow depth was greater than 0.1 m, 0.2 m, or 0.3 m over the coarse of each debris-flow event varied significantly between large and small transport events (Table. 2). The total time elapsed while the measured flow depth was greater than 0.1 m, 0.2 m, or 0.3 m was largest for the 15 September event. Although the 6 September event had surges of comparable depth to the 15 September event, there were fewer surges and the shallow flow between surge fronts only lasted for a short time. The short duration of shallow flow observed during the 6 September event is in strong contrast to the 15 September event where there were sustained periods of flow greater than 0.1 m between the deeper surge fronts. This indicates that total event volume can be strongly influenced not only by the largest surges, but also by sustained periods of moderate flow.

For the two larger events, September 6 and September 15, we observed changes in surge characteristics as the flows moved downstream past the three stations (Fig. 5 and 6). The coalescence of small surges into larger, longer-duration surges is particularly pronounced in the 6 September event (Fig. 5C). During the 15 September event, the opposite behavior occurred after 17:50. At this time, flows measured at the upper and middle stations became water-dominated and lacked the deep surge fronts measured during the previous 10 minutes. However, by the time these moderate-depth, water-dominated flows reached the lower station, deep surges had developed (Fig. 6). Although there was a range in surge depth (0.31 m to 1.1 m at the upper station) almost all surges had the asymmetric shape characteristic of debris flows, with a steep and deep front followed by a more gently decreasing tail.

TOTAL NORMAL BASAL STRESS

Total normal basal stress varied in phase with stage, with no consistent time lag observed between changes in stage and changes in stress. Assuming a one-dimensional static stress state, we calculated that the mean wet bulk densities of the flows ranged between 1400 and 2200 kg/m3 (see MCCOY *et al*., 2010 for an explicit density time series). We measured denser mixtures near the surge front (1800-2200 kg/m3), and less dense mixtures in the water-dominated tails (1400-1800 kg/m3). A similar range of densities have been measured in other field and large-scale laboratory measurements of passing debris flow surges (PIERSON, 1986; MCARDELL *et al*., 2007; IVERSON *et al*., 2010)

PORE-FLUID PRESSURE AND SOIL MOISTURE

Over the four different debris-flow events, the pore-fluid pressure measured at the sediment-bedrock interface was variable and depended largely on the thickness of overlying bed sediment and the state of saturation of the bed sediment. For the majority of the events, no pressure response due to the pressure head of the overriding flow was measured (presumably because the static bed sediment between the overriding debris flows and the pressure transducer at the bedrock-sediment interface was partially dry). When there was no bed sediment covering the pressure transducer

and the flow interacted directly with the transducer (such as during the end of the event on the 15 September) we measured large spikes in pore-fluid pressure. Only during the 2 June event did we measure a significant pressure response beneath some thickness of bed sediment. During this event, positive pore-fluid pressures were developed in the static bed sediment at the upper and middle stations prior to the first surge front arriving. At the upper station, we measured an attenuated pressure signal that generally followed the trend of flow stage, but sharp increases in pore-fluid pressure lagged sharp increases in stage and normal stress by 4-8 s (Fig. 3B). We presume the pressure signal was muted because the bed sediment may not have been complete saturated. From video observations, it was evident that the measured lag between increases in stage and increases in pore-fluid pressure was equal to the time the coarse-grained, visually unsaturated front spent traveling over the sensors. Similar lags between the rise in stage and the rise in pore-fluid pressure have been repeatedly measured in large-scale laboratory debris flows and related to the passage of the dilated, coarse grain granular front (IVERSON *et al*., 2010). At the middle station during the 2 June event, we measured a less attenuated pressure signal and peak measured pressures were up to two times hydrostatic (MCCOY et al., 2010, Fig. 3C).

Volumetric water content (i.e. soil moisture) measured at depths of ~5 cm and ~45 cm in the channel sediment ~50 m downstream of the middle station, where total sediment depths were greater than 2 m, remained unchanged from the pre-storm values of ~10% and 13%, respectively, during the short duration storms of 26 July, 6 and 15 September (Table. 2). During the longer duration 2 June event soil moisture increased from 15% to 18% at 5 cm, and hours after the end of the flow event we measured soil moistures > 30% at 45 cm depth. Our measurements indicate that relatively dry bed sediments are typical of storms in which the duration is short relative to the infiltration time. Only during longer duration storms and only locally where the bed sediment was thin and surrounded by large areas of bedrock (as was characteristic of the upper and middle station) did sediments approach saturation. The June 2 event also indicates that merely having a saturated or nearly saturated bed (as was locally present at both the upper and middle station) does not ensure entrainment. The June 2 event was depositional at both stations where the shallow bed sediments were locally saturated.

SUMMARY AND CONCLUSIONS

Using a combination of PIT tagged tracer rocks, automated monitoring, and terrestrial laser scanning, we measured the entrainment and transport response of the four debris-flow events that occurred at Chalk Cliffs in the summer of 2009. We also constrained the rainstorm characteristics, topographic parameters, and flow properties that were responsible for the observed responses. All the observed debris flows were trigged by storms capable of generating surface-water runoff. These storms generally had durations of less than two hours, but variable intensities (10 – 40 mm/hr). The arrival of debris-flow surges generally followed the onset of rain by less than one hour. All flow events consisted of multiple surges, with each asymmetric surge composed of a steep granular front and a more watery tail. Despite these similarities, the four events in the summer of 2009 were surprisingly variable in terms total volume and, especially, runout length, and volume of entrained bed sediment. The 15 September event was conspicuously larger by these measures than the preceding three flows.

Using PIT tagged tracer rocks we quantified the large variability in particle transport distance and found a strongly bimodal transport response. In the short-transport mode, the population of tracer particles had transport distances in which both the mean and maximum distances were generally tens of meters and the tracers only travelled a small fraction of the debris-flow dominated catchment length. In the contrasting long-transport mode, the population of tracer particles had mean and maximum travel distances on the order of thousands of meters and the majority of the population travelled the entire length of the catchment during a single flow event.

TLS surveys (presented in the companion paper by STALEY et al.) taken before and after flow events showed little change in reach-scale topographic parameters over the course of the summer. Therefore, the large variation in observed transport and entrainment response must be controlled by individual storm characteristics and flow properties, rather than by changes in flow-path topography.

Large-entrainment, long-transport flows were best differentiated from small-entrainment, short-transport flows by peak 10-minute rain intensity, total elapsed time with flow of significant depth in the channel, and to a lesser extent, peak surge depth and velocity. Larger events had higher 10-minute rain intensities and during these higher intensities (20-40 mm/hr) a larger fraction of the precipitation exited the basin as measurable debris-flow surges and overland flow. The 15 September event had the longest elapsed time during

which flow depths were measurable (>0.1m), and the longest elapsed time during which flow depths were deep (>0.3 m), in addition to having the most rapidly moving surge fronts. With a growing dataset of events in which both the effects of the debris-flow event and the triggering rainstorm and flow properties are quantified it will be possible to test the strength of these correlations and gain additional insight into the controlling mechanisms of initiation, entrainment, and transport by debris flows in natural, uncontrolled settings.

ACKNOWLEDGEMENTS

This research was supported by the National Science Foundation (NSF) Graduate Fellowship, NSF grants EAR-0643240 and 0934131, NSF CAREER grant 0239749, and the U.S. Geological Survey Landslide Hazards Program. ALSM data was provided by NCALM. We thank Joe Gartner, for field assistance and Nate Bradley for advice and technical help with the RFID survey equipment. Careful reviews on an earlier version of the manuscript by Mark Reid and Nate Bradley improved the clarity of presentation.

REFERENCES

ARATTANO, M. & MARCHI, L. (2000) - *Video-derived velocity distribution along a debris flow surge*. Physics and Chemistry of the Earth Part B, **25**(9), 781-784.

BERTI, M, & SIMONI, A. (2005) - *Experimental evidences and numerical modeling of debris flow initiated by channel runoff*. Landslides, **2**(3), 171–182.

BERTI, M., GENEVOIS, R., LAHUSEN, R., SIMONI, A., & TECCA, P. R. (2000) - *Debris flow monitoring in the Acquabona watershed on the Dolomites (Italian Alps)*. Physics and Chemistry of the Earth Part B-Hydrology Oceans and Atmosphere, **25**(9), 707–715.

BRADLEY, D. N. (2010) - *Modeling Sediment Transport with Random Walks*. PhD thesis, University of Colorado, Boulder, Colorado, USA.

CANNON, SH, KIRKHAM, RM, & PARISE, M. (2001) - *Wildfire-related debris-flow initiation processes, Storm King Mountain, Colorado.* Geomorphology, **39**(3-4), 171–188.

COE, J.A., KINNER, D.A., & GODT, J.W. (2008) - *Initiation conditions for debris flows generated by runoff at Chalk Cliffs, Central Colorado*. Geomorphology, **96**(3-4), 270–297.

COE, JEFFREY A., KEAN, JASON W., MCCOY, SCOTT W., STALEY, DENNIS M., & WASKLEWICZ, THAD A. (2010) - *Chalk Creek Valley: Colorado's natural debris-flow laboratory*. In: Morgan, L.A., & Quane, S (eds), Through the Generations: Geologic and Anthropogenic Field Excursions in the Rocky Mountains from Modern to Ancient: Geological Society of America Field Guide 18. The Geological Society of America.

FRYXELL, F.M., & HORBERG, C.L. (1943) - *Alpine mud flows in Grand Teton National Park, Wyoming*. Bulletin of the Geological Society of America, **54**(3), 457.

IVERSON, R. M., LOGAN, M., LAHUSEN, R. G., AND BERTI, M. (2010) - *The perfect debris flow? Aggregated results from 28 large-scale experiments*. Journal of Geophysical Research, 115(F3):F03005.

LARSEN, I.J., PEDERSON, J.L., & SCHMIDT, J.C. (2006) - *Geologic versus wildfire controls on hillslope processes and debris flow initiation in the Green River canyons of Dinosaur National Monument*. Geomorphology, **81**(1-2), 114–127.

MCARDELL, B. W., BARTELT, P., AND KOWALSKI, J. (2007) - *Field observations of basal forces and fluid pore pressure in a debris flow*. Geophysical Research Letters, **34**(7).

MCCOY, S. W., KEAN, J. W., COE, J. A., STALEY, D. M., WASKLEWICZ, T. A., & TUCKER, G. E. (2010) - *Evolution of a natural debris flow: In situ measurements of flow dynamics, video imagery, and terrestrial laser scanning*. Geology, **38**, 735–738.

MEYER, G.A., WELLS, S.G., & TIMOTHY JULL, AJ. (1995) - *Fire and alluvial chronology in Yellowstone National Park: Climatic and intrinsic controls on Holocene geomorphic processes*. Geological Society of America Bulletin, **107**(10), 1211.

MILLER, MARTIN G. (1999) - *Active breaching of a geometric segment boundary in the Sawatch Range normal fault, Colorado, USA*. Journal of Structural Geology, **21**(7), 769–776.

PIERSON, T.C. (1986) - *Flow behavior of channelized debris flows*, *Mount St. Helens, Washington,* In Abrahms, A.D., (ed.), Hillslope Processes, Allen and Unwin, Boston, 269-296.

STALEY, DENNIS M., WASKLEWICZ, THAD A., COE, JEFFREY A., KEAN, JASON W., MCCOY, SCOTT W., & TUCKER, GREG E. *Observations of debris flows at Chalk Cliffs, Colorado, USA: Part 2, changes in surface morphometry from terrestrial laser scanning in the summer of 2009*. In: Debris-Flow Hazards Mitigation: Mechanics, Prediction and Assessment, vol. This volume.

SUWA, H., OKUNISHI, K., AND SAKAI, M. (1993) - *Motion, debris size and scale of debris flows in a valley on Mount Yakedake, Japan*, In Sediment Problems: Strategies for Monitoring, Prediction and Control, IAHS Publ. no. 217, 239-248.

TUCKER, G. E. AND BRADLEY, D. N. (2010) - *Trouble with diffusion: Reassessing hillslope erosion laws with a particle-based model.* Journal of Geophysical Research, 115:F00A10.

VANDINE, DF. (1985) - *Debris flows and debris torrents in the southern Canadian Cordillera*. Canadian Geotechnical Journal, **22**(1).

WOHL, E.E., & PEARTHREE, P.P. (1991) - *Debris flows as geomorphic agents in the Huachuca Mountains of southeastern Arizona*. Geomorphology, **4**(3-4), 273–292.